Q. J. R. Meteorol. Soc. (2004), **130**, pp. 1137–1151 doi: 10.1256/qj.03.52

Describing surface fluxes in katabatic flow on Breidamerkurjökull, Iceland

By O. PARMHED[1]*, J. OERLEMANS[2] and B. GRISOGONO[1]
[1]*Stockholm University, Sweden*
[2]*Utrecht University, The Netherlands*

(Received 21 March 2003; revised 20 October 2003)

SUMMARY

For very stable boundary layers there is no well-accepted theory today. In this study, an improved Prandtl model with varying diffusivity is applied to less than ideal conditions for pure katabatic flow pertaining to very stable boundary layers. We find that the improved Prandtl model adequately describes the usual and persistent katabatic glacier wind on Breidamerkurjökull. This is true even for flows with very different heights and strengths of the jet. A theoretical estimate of the katabatic jet height, based on temperature deficit and lapse rate, is verified. The calculated surface fluxes compare well with the measured turbulence parameters. A possible reason for the robustness of the katabatic jet (and other low-level jets) is given in terms of the Scorer parameter.

KEYWORDS: Glacier wind Low-level jet Very stable boundary layer WKB method

1. INTRODUCTION

The present interest in climate change and its consequences such as sea-level rise and glacier melting has highlighted our need for a better understanding of the stable boundary layer (SBL). Although SBLs are common, perhaps most so as the nocturnal boundary layer, they are still poorly understood and not well described in numerical weather and climate models. Mahrt (1998) identified two forms of SBL. The classic, weakly stable boundary layer, similar to the nocturnal SBL, is the focus of most SBL studies. Within the weak SBL, Monin–Obukhov (MO) theory is usually applicable. MO theory is used in most numerical models for their boundary-layer treatment. However, in the case of very stable boundary layers (VSBL), the MO theory often underestimates the surface fluxes. Mahrt concludes that more data are needed on the VSBL to understand them better and to model them accurately. From analysis of a dataset covering almost five orders of magnitude in the stability parameter (z/L, where L is the MO length), Pahlow *et al.* (2001) found that the MO 'concept does not hold in general'.

A second possible reason for the failure of the MO theory is the surface slope. MO theory assumes that buoyancy acts only in the vertical (Munro and Davies 1978). The sloping surface means that buoyancy will enter the horizontal momentum equation. This buoyancy, acting on the horizontal momentum, is also the driving force behind the katabatic flow. An additional aspect of the katabatic flow is the presence of a low-level jet. This jet is typically positioned at a height, z_j, below about 10 m, often placing it well below the MO length, leaving MO theory invalid because there is a shorter important length-scale present ($z_j < L$). This low-level jet in the katabatic flow means that, although friction acts at the surface, the production of turbulence is not dominated by the surface but is strongly influenced by the jet (e.g. van der Avoird and Duynkerke 1999).

Over sloping surfaces, katabatic flow is a ubiquitous feature of VSBLs (e.g. Stull 1988; Egger 1990). Field experiments have shown that in the VSBL over land ice, katabatic flows are usual and persistent (e.g. Oerlemans *et al.* 1999). Glacier melting is most sensitive to changes in the long-wave radiation and the turbulent heat flux (e.g. Oerlemans 2001). The properties of the katabatic VSBL are important for the understanding

* Corresponding author: Department of Meteorology, Stockholm University, S-106 91 Stockholm, Sweden.
e-mail: oskar@misu.su.se

of glacier response to climatic changes. In view of the referenced inapplicability of the MO theory for the shallow katabatic boundary layer, we need to look elsewhere for a solution.

The simplest description of a katabatic flow is given by the Prandtl model for gravity-driven flow down a cooled inclined surface (Prandtl 1942; Defant 1949; Mahrt 1982). The simplicity of the Prandtl model and the fact that it is analytical makes it attractive for understanding the pure katabatic flow. However, the model has some significant drawbacks. Perhaps the most serious problem with the Prandtl model (when considering surface fluxes) is its inability to describe correctly the sharp near-surface gradients in temperature and wind that are often observed (Defant 1949; Munro 1989; Fig. 3.5 of Egger 1990; Oerlemans 1998). Conversely, above the jet the simulated gradient is often too sharp compared with observations (Oerlemans 1998; Denby 1999). These weaknesses of the model are due to the use of a constant value for the eddy diffusivity that is necessary for the model to be analytically solvable. A more complex form of analysis is Large Eddy Simulation (LES). Although LES techniques have evolved significantly over recent years, we are not aware of any successful LES of steady shallow katabatic flow. The work by Skyllingstad (2003) is an important step, but it deals only with evolving katabatic flow.

Recently, Grisogono and Oerlemans (2001a,b, hereafter GOa,b) showed that the Prandtl model can be improved if a varying assigned eddy diffusivity profile, $K(z)$, is used instead of a constant value. They use the WKB† method (e.g. Bender and Orszag, 1999) to allow $K(z)$ to vary with height.

In this study we use data from the glacio-meteorological field experiment on Vatnajökull, Iceland, during the summer of 1996, to verify the ability of the modified Prandtl model to simulate the near-surface gradients of the katabatic flow. This was undertaken in less than ideal conditions and in an environment very different from that of GOa, although still addressing the flow over land ice. In doing this, we also confirm the applicability of the eddy diffusivity profile suggested in GOa, and verify the theoretical estimate of the height of the katabatic jet. We also compare the calculated and measured surface fluxes.

Besides the persistence of the pure katabatic flow, we also note a dynamically induced decoupling of the katabatic jet from the higher layers. This hints at a theoretical explanation of the robustness of low-level jet flows in diverse environments (e.g. Burk *et al.* 1999).

2. The katabatic flow model

The classic Prandtl model describes the katabatic flow down a cold inclined surface (or anabatic flow up a warm inclined surface). It equates the divergence of the turbulent fluxes of momentum and heat to the advected background temperature lapse rate and the buoyancy acceleration (Prandtl 1942; Mahrt 1982; Egger 1990; Grisogono and Oerlemans 2002, hereafter GOc):

$$\frac{\partial \theta}{\partial t} = -\gamma u \sin(\alpha) - \frac{\partial(\overline{w'\theta'})}{\partial z} \tag{1}$$

$$\frac{\partial u}{\partial t} = g\frac{\theta}{\theta_0}\sin(\alpha) - \frac{\partial(\overline{w'u'})}{\partial z}. \tag{2}$$

† After Wentzel, Kramers and Brillouin, who popularized the method in theoretical physics. Sometimes also referred to as WKBJ, including Jeffreys who, together with Rayleigh, contributed to its early development. The original approximation was really made independently by Liouville and Green in 1837.

In (1) and (2), θ is the potential temperature perturbation (i.e. actual potential temperature minus background potential temperature), θ_0 is a reference temperature (typically the melting point of ice), γ is the background potential temperature lapse rate, α is the slope of the surface and $\overline{w'\theta'}$ and $\overline{w'u'}$ are turbulent heat and momentum fluxes parametrized with the K-theory according to:

$$\overline{w'\theta'} = -K\frac{\partial\theta}{\partial z}, \quad \overline{w'u'} = -KPr\,\frac{\partial u}{\partial z}, \tag{3}$$

where K is the eddy difusivity for heat and Pr is the turbulent Prandtl number. Under steady-state conditions (the time-dependent case is addressed in Grisogono (2003)) and assuming that K and Pr are constants, the single governing equation resulting from (1)–(3) becomes (Prandtl 1942):

$$\frac{\mathrm{d}^4\theta}{\mathrm{d}z^4} + N^2\frac{\sin^2(\alpha)}{Pr\,K^2}\theta = 0, \tag{4}$$

$$\text{where } N = \sqrt{\frac{g\gamma}{\theta_0}}.$$

If $K = K(z)$ the equation becomes somewhat more complicated:

$$\underbrace{\frac{\mathrm{d}^4\theta}{\mathrm{d}z^4}}_{\text{0th order}} + \underbrace{\frac{4}{K(z)}\frac{\mathrm{d}K}{\mathrm{d}z}\frac{\mathrm{d}^3\theta}{\mathrm{d}z^3}}_{\text{1st order}} + \underbrace{\left\{\frac{3}{K(z)}\frac{\mathrm{d}^2K}{\mathrm{d}z^2} + \frac{2}{K(z)^2}\left(\frac{\mathrm{d}K}{\mathrm{d}z}\right)^2\right\}\frac{\mathrm{d}^2\theta}{\mathrm{d}z^2} + \left\{\frac{1}{K(z)}\frac{\mathrm{d}^3K}{\mathrm{d}z^3} + \frac{1}{K(z)^2}\frac{\mathrm{d}K}{\mathrm{d}z}\frac{\mathrm{d}^2K}{\mathrm{d}z^2}\right\}\frac{\mathrm{d}\theta}{\mathrm{d}z}}_{\text{higher order}} + \underbrace{N^2\frac{\sin^2(\alpha)}{Pr\,K(z)^2}\theta}_{\text{0th order}} = 0, \tag{5}$$

where the 0th order terms first appear in (4). Hence (5) indicates the perturbation analysis used and the order of balance of the terms in the model (GOa,c).

Following GOa,c, an approximate solution to (5) can be found using the WKB method for given α, γ and $K(z)$. The validity of the WKB method depends on how slowly K varies with z; a justification for the use of the WKB method for katabatic flows can be found in GOc. The requirement for the K profile to be smooth restricts calculations to a K profile that has no sharp gradients. In this work, the linear-Gaussian K-profile of GOa is used:

$$K(z) = \frac{K_{\max}\,\mathrm{e}^{\frac{1}{2}}}{H_K}\cdot z\cdot \mathrm{e}^{-\frac{1}{2}(z/H_K)^2}. \tag{6}$$

GOb,c show that the maximum value, $K_{\max}$, of $K(z)$ can be obtained from WKB theory through the expression

$$K_{\max} \approx 32N\alpha z_{\mathrm{j}}H_K\frac{1}{\pi^2\sqrt{\mathrm{e}Pr}}, \tag{7}$$

$$\text{with } H_K = \max(2z_{\mathrm{j}},\, z_{\mathrm{i}}),$$

where $N_\alpha = N \sin(\alpha)$, H_K is the height of the maximum diffusivity and z_i is the inversion height. However, the diffusivity can also be related to the height and strength of the katabatic jet, since the latter is a very important, perhaps determining, factor for the local turbulence (e.g. van der Avoird and Duynkerke 1999). Following this line of reasoning and using $K_\mathrm{max} = \mathrm{const} \cdot H_\mathrm{SBL} \cdot \max(u)$ as in Oerlemans (1998) and GOc, z_j can be found as

$$z_\mathrm{j} = B \cdot \frac{-C}{\gamma \sqrt{\sin(\alpha)}}, \tag{8}$$

where C is the potential temperature deficit at the surface, H_SBL is the SBL height and B is a coefficient. If the relation (8) can be validated, this would tie in the background parameters determining z_j such that the model input would consist of α, γ, C and Pr, together determining the katabatic flow. Otherwise the model input remains α, γ and $K(z)$. To sum up, using $K \sim z_\mathrm{j} \cdot N_\alpha \cdot H_k$ and $K \sim H_\mathrm{SBL} \cdot \max(u)$, we relate $K(z)$ to z_j and the background parameters in (8). In an effort to verify (8) to observations, we will give a first estimate of the coefficient B in section 4.

For sufficiently smooth variability in the K profile, the first and fourth (0th order) terms on the left-hand side of (5) dominate. The solution is split into two parts, one inner (between the surface and H_K) and one outer (above H_K). The two solutions are then patched at the point of intersection. The higher order corrections, that are difficult to compute and do not necessarily improve the overall result, are neglected. For a given input of α, γ, C, Pr, the profiles of u and θ can now be computed:

$$u_\mathrm{inner} = -C\mu \cdot \mathrm{e}^{-I(z)} \cdot \sin\{I(z)\} \tag{9}$$

$$\theta_\mathrm{inner} = C \cdot \mathrm{e}^{-I(z)} \cdot \cos\{I(z)\} \tag{10}$$

$$(u, \theta)_\mathrm{outer} = (u, \theta)_\mathrm{inner} \cdot \left\{ \frac{K(z)}{K_\mathrm{max}} \right\}^{-\frac{1}{4}}, \tag{11}$$

$$\text{where } I(z) = \sqrt{\frac{\sigma_0}{2}} \int_0^z \frac{1}{\sqrt{K}}\,\mathrm{d}z, \quad \mu = \sqrt{\frac{g}{\theta_0 Pr\,\gamma}}$$

$$\text{and } \sigma_0 = \sqrt{\frac{g\gamma\,\sin^2(\alpha)}{Pr\,\theta_0}} = \frac{N_\alpha}{\sqrt{Pr}}.$$

3. Observations

The data used in this study were obtained during the 1996 field campaign on Vatnajökull, Iceland. The campaign is described in detail in Oerlemans *et al.* (1999). During the campaign several weather stations were located both on and off the ice. Stations were concentrated on Breidamerkurjökull, a large outlet glacier flowing down to the Atlantic, close to 64°05′N, 16°19′W (Fig. 1). Helium balloons were used to obtain profiles through the lowest 500 m of the atmosphere.

The near-surface data presented here are hourly averages from the ∼9 m wind mast at station A4 (see Oerlemans *et al.* 1999) at the lower part of Breidamerkurjökull (see Fig. 1). Wind and temperature were measured at five levels, different for the two variables. Connecting these data to the balloon soundings, which are unreliable near the ground, gives a good picture of the vertical profile of wind and temperature. Also, a sonic anemometer was used to measure turbulence statistics (e.g. van der Avoird and Duynkerke 1999) at a height of ∼3 m.

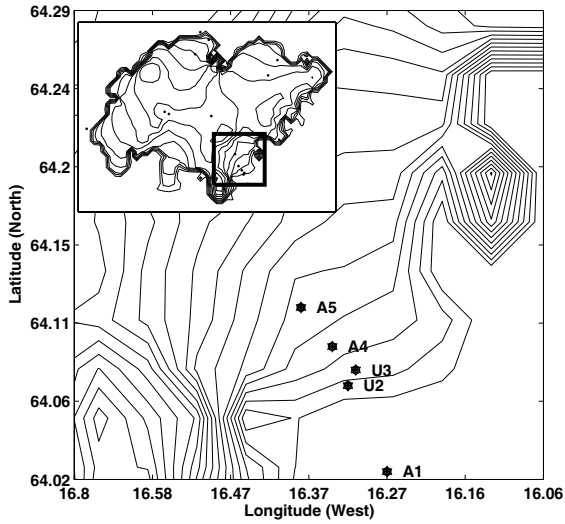

Figure 1. Topographic map of the Vatnajökull glacier, Iceland, with the locations of weather stations from the 1996 field campaign. Expanded section shows Breidamerkurjökull. Height contour interval is 100 m, starting at zero at lower right.

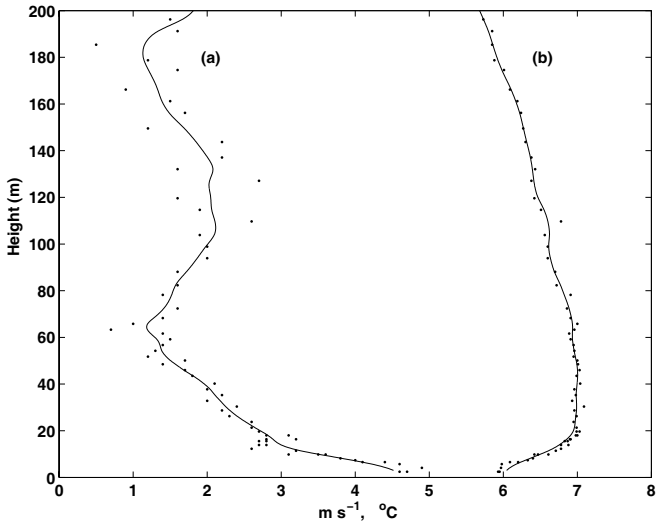

Figure 2. Examples of (a) wind and (b) temperature profiles from balloon ascents. Dots indicate raw data and solid lines the filtered profiles.

Balloons were launched from two positions (stations U2 and U3, see Oerlemans *et al.* 1999), some 1300 and 500 m respectively downstream of the profile mast. Until 11 June, the launch site was located off the ice at the end of Breidamerkurjökull, and thereafter at site U3 on the ice.

The height of the balloon observations was not measured directly but was calculated from the pressure and temperature data assuming hydrostatic balance. Because the balloon data were noisy, a digital filter was used. Since the filter required a constant sample rate, the data were linearly interpolated onto a 2 m vertical grid, this being the

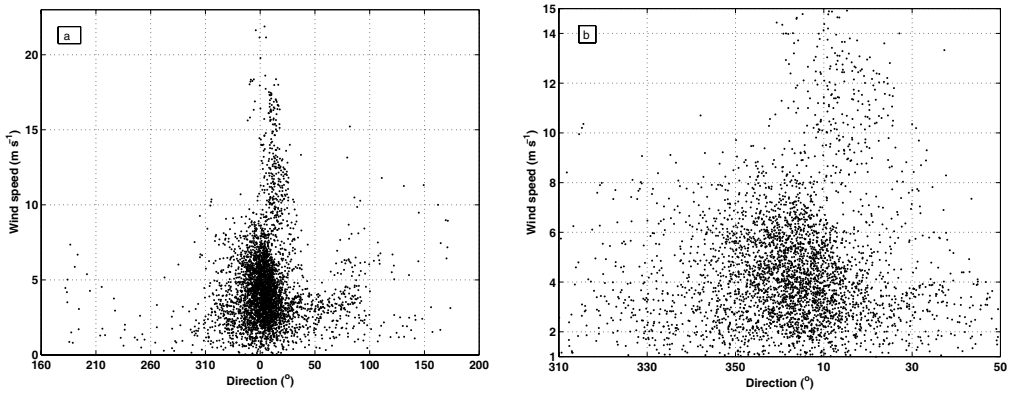

Figure 3. (a) Scatter plot (4944 data points) of wind direction versus wind speed (hourly means) at Vatnajökull for the entire summer field campaign 1996. Wind speed is taken from the uppermost anemometer at approx. 9 m height, and wind direction from a wind vane at the top of the mast. (b) shows an enlargement of the centre portion of (a).

smallest vertical increment in the data. This was done to retain as much data as possible while feeding as few non-measured points as possible to the filter. The filter was the commercial Matlab program using its first-order Butterworth filter with a 20 m cutoff (see Emery and Thomson 1997). This cutoff is twice the largest vertical increment in the data (cf. the Nyqvist frequency) to avoid aliasing. The raw wind speed and temperature data and the filtered profiles for one example sounding are shown in Fig. 2.

4. Results

(*a*) *Data*

To show how common katabatic flows are over Breidamerkurjökull, Fig. 3(a) displays the observed wind speed and direction for May–August from the uppermost anemometer/vane (≈9 m) on the wind mast at station A4. Figure 3(b) shows an enlargement, focusing on the majority of the winds; it contains ∼75% of all the data points, showing that the flow was highly unidirectional. Considering the surrounding environment—a melting glacier—and the fact that the persistent wind direction was down-slope, we assume this flow to be katabatic (Oerlemans *et al.* 1999). Further, simple but conservative criteria for pure katabatic flow were used, requiring a local wind maximum somewhere below the uppermost anemometer (≈9 m) and temperature at the mast strictly increasing with height. The number of cases thus identified as purely katabatic did not depend on the wind direction. 45% of data from station A4 conform to these criteria. In reality, there were probably more katabatic flow occurrences (e.g. Mahrt 1982; Egger 1990), since the criteria reject all flows with a wind maximum above ≈6 m (the height of the second highest anemometer).

Figure 4 shows a time–height plot of the wind speed from the balloon soundings (raw unfiltered data). The soundings are not equally spaced in time, although they are in consecutive order. The abscissae shows the ordinal number of the sounding, the ordinate shows the height and the grey-scale shows the average wind speed in 5 m bands in the vertical. It is readily seen that a low-level jet was present in the vast majority of the soundings. This is a further independent evidence of persistent katabatic flows. A second set of criteria for pure katabatic flow, similar to that used for the wind mast data, was applied to the balloon data: a wind maximum within the lowest 15 m, a strictly

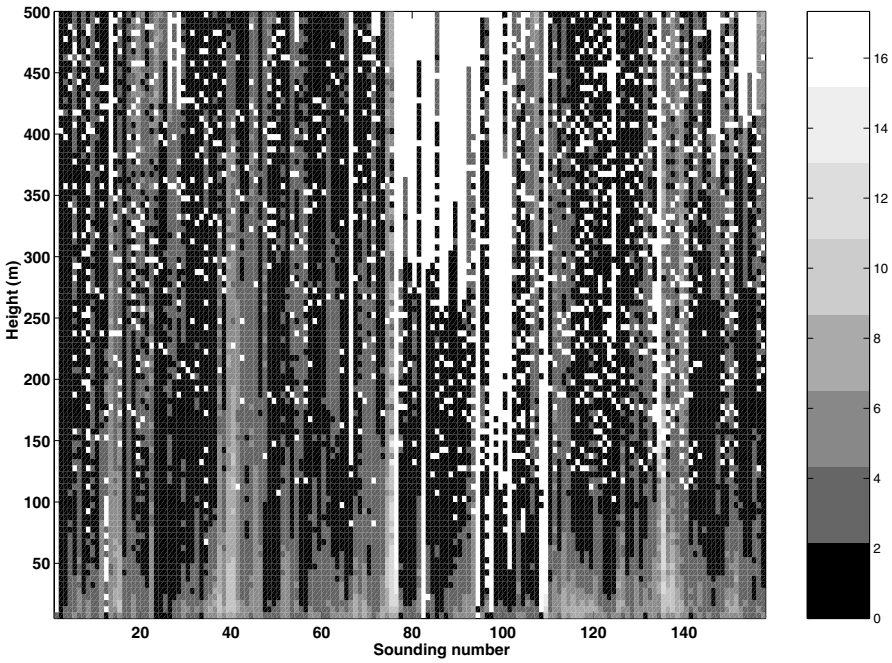

Figure 4. Wind speeds in a sample of soundings from the 1996 field campaign, with speeds according to the grey-scale. White (the strongest wind speed) also indicates lack of data, but this is of no consequence near the ground due to the limited wind speeds there.

increasing temperature over the same distance and a down-slope wind direction. 40% of the available balloon soundings conform to these conditions and so can be considered as purely katabatic. As with the wind mast data, there were probably more katabatic flow regimes than those identified by using these crude and pragmatic criteria.

Because the ice on the glacier was melting irregularly during the observations, the surface roughness also changed. According to Smeets *et al.* (1999), the size of the roughness elements at station A4 was in the range of 0.25 m to slightly above 1 m. For this reason, we further excluded from these data all cases with a jet maximum below 2 m. It is not likely that a jet elevated above the ground less than twice the roughness length would act as a well-defined steady katabatic flow.

The mast and sounding data do not always agree; one may show katabatic flow according to the above criteria while the other does not. Although this may sound critical of the criteria it is actually easily explained. The mast data are one-hour averages of the variables while the balloon soundings are instantaneous values. Also, there is a horizontal separation between the mast and balloon sounding locations.

Out of a total of 158 soundings, 40 (i.e. 25%) show katabatic flow from both observation systems according to the above criteria. In addition, some flows deemed katabatic from the soundings are not deemed katabatic from the mast data, i.e. flows with localized maxima above the top of the observing mast. For comparison, a number of such soundings were added to the following analysis.

Figure 5 shows a selection of soundings with the corresponding mast observations. The sample is randomly chosen (using the 'rand' function in the Perl scripting language) from those soundings that were deemed katabatic. In addition, 10 soundings are added where the katabatic jet derived from balloon soundings was located above the second

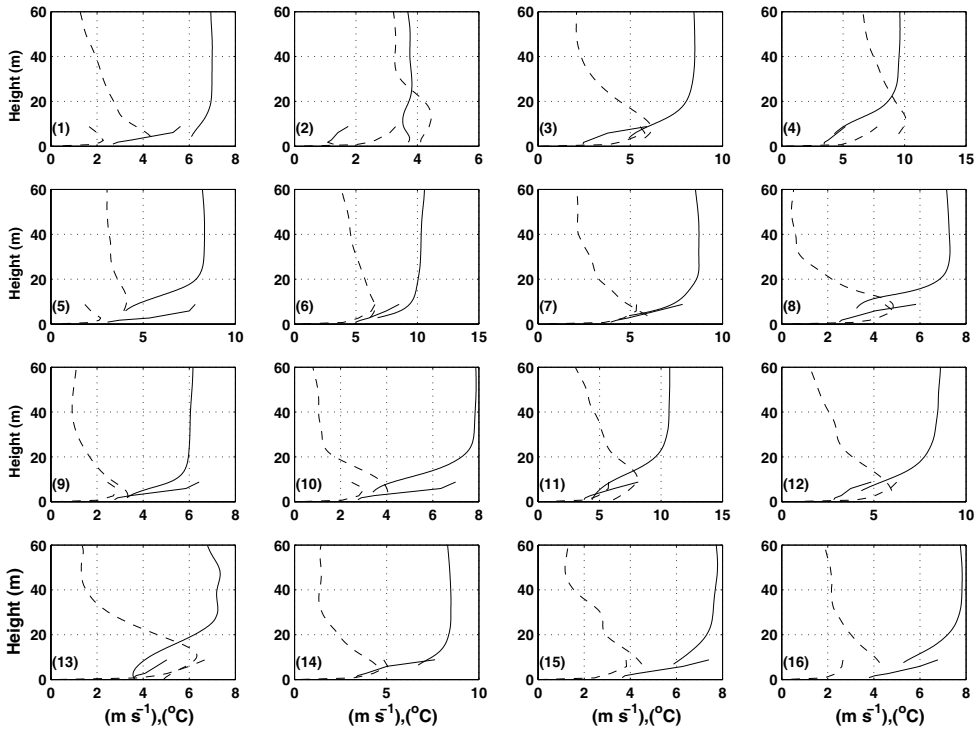

Figure 5. Composite (mast and balloon) plots of wind speed (dashed) and temperature (solid) for the times listed in Table 1.

highest anemometer on the observation mast. This yields a total of 50 soundings, or 32% of all soundings.

Table 1 summarizes the characteristics for the soundings in Fig. 5. Variables z_j, u_j, γ and z_i are taken from the balloon soundings. Also shown in Table 1 are the values of K_{max} and H_K calculated from (8) and (9), using $\alpha = 4°$ and $Pr = 1$. As usual for many VSBL, the inversion height is difficult to determine (e.g. Grisogono *et al.* 1998; Mahrt 1998; GOc) and is therefore accompanied by '?' in Table 1 to mark this uncertainty. Here, the inversion height is arbitrarily defined as the height where $\partial\theta/\partial z = 0.01$ K m^{-1}. The temperature deficit, C, is calculated as the difference between the background lapse rate intersection with the surface, and the surface temperature. (It is assumed that the glacier surface has a temperature of 0 °C, since the glacier is melting all through the summer).

Regarding Table 1, it may be noted that the MO length, L, calculated from the profiles below 4 m height is 12 ± 8 m, i.e. two to three times larger than z_j (not counting the uncertainty). This is a sign that L is indeed not the relevant length-scale for the katabatic flow.

Several observations presented in Fig. 5 show a mismatch between the top of the mast and the bottom of the balloon sounding. Part of this mismatch is due to calculation of the balloon height assuming that the air is in hydrostatic balance. In reality, the noise in the start of the sounding means that the absolute height of the balloon can be questioned. The soundings also show differences in the magnitudes of the measured variables. These differences are most probably due to the horizontal separation of the

TABLE 1. DATA FROM THE 1996 FIELD CAMPAIGN ON THE VATNAJÖKULL GLACIER FOR THE SOUNDINGS SHOWN IN FIG. 1. SEE TEXT FOR DETAILS.

		Observed					Calculated	
No.	Date; Time (LST)	$-C$ (°C)	γ (K m^{-1})	z_j (m)	z_i(?) (m)	u_j (m s^{-1})	H_K (m)	K_{max} (m^{2}s^{-1})
1	25/5; 17.35	7.0	0.0035	4.2	19.0	4.3	19.0	0.124
2	27/5; 08.50	4.0	0.0025	13.0	27.8	4.4	27.8	0.470
3	09/6; 08.36	8.0	0.0018	7.8	29.1	6.2	29.1	0.252
4	11/6; 14.00	9.5	0.0044	11.7	30.2	10.1	30.2	0.611
5	14/6; 11.40	8.3	0.0062	10.6	26.8	4.1	26.8	0.583
6	14/6; 23.39	10.0	0.0062	7.5	61.0	6.6	61.0	0.936
7	15/6; 02.38	8.7	0.0089	3.7	22.7	5.9	22.7	0.210
8	07/7; 02.41	7.3	0.0057	8.0	27.2	4.8	27.2	0.428
9	07/7; 05.39	5.9	0.0095	2.5	18.0	3.3	18.0	0.116
10	07/7; 16.36	7.8	0.0048	4.2	27.7	4.0	27.7	0.212
11	20/7; 17.33	10.8	0.0044	10.3	33.8	8.1	33.8	0.602
12	21/7; 02.45	8.4	0.0057	4.9	31.6	6.0	31.6	0.299
13	21/7; 05.36	7.3	0.0072	10.7	29.7	6.3	29.7	0.712
14	11/8; 17.33	8.5	0.0062	6.4	22.9	4.4	22.9	0.301
15	28/8; 11.31	7.5	0.0071	6.9	25.9	4.5	25.9	0.389
16	28/8; 14.32	7.8	0.0063	7.5	31.3	4.2	31.3	0.484

sites and the fact that the balloon data are instantaneous while the mast data are hourly averages.

(*b*) *Model*

Using the values of H_K, K_{max} and the various observed variables from Table 1, the improved Prandtl model was used to calculate profiles of wind and temperature. The results from these calculations are presented in Table 2. The correspondence between model results and observations is shown on scatter plots in Fig. 6. Both the height (only the soundings in Tables 1 and 2) and strength of the jet maximum (all 50 data points) are shown. The jet heights, z_j, are shown for three different values of Pr. It is clear that in this flow the relevant Pr is unity or just above, similar to that reported by Mahrt (1998) for the Microfronts experiment. It is also clear from Fig. 6 that an increase in Pr results in a reduced slope for the regression of calculated versus observed z_j. Considering that z_j is perhaps the most important factor in determining the near-surface turbulence (e.g. van der Avoird and Duynkerke 1999; GOc), the agreement in Fig. 6 is satisfactory. In view of this correspondence, the rest of this study will use $Pr = 1$. The agreement for u_j is weaker, showing a large scatter, with a distinctive tendency for the model to overestimate the wind speed. Presuming that the model is not in error, the scatter of u_j in Fig. 6 is assumed to depend on the uncertainty in determining C, given the high sensitivity of the wind speed to C.

(*c*) *Determining the jet height*

Equation (8), suggested in e.g. GOc and Oerlemans and Grisogono (2002), is a theoretical estimate of z_j. Although not new, the relation has not been tested versus observations and no effort has been made to quantify the coefficient B. In this section, we make an estimation of B and compare the result to the observations.

Using the observed value of z_j from the 50 soundings in (8), the mean value of the coefficient B is found to be $(9.7 \pm 5.7) \times 10^{-4}$. Figure 7 shows a scatter plot of the observed values of z_j versus those calculated from (8) using this value of B; there is a scatter around the 1:1 line, as in Fig. 6. The high density of data points located in two

TABLE 2. MODEL RESULTS CORRESPONDING TO OBSERVATIONS IN TABLE 1, CALCULATED BY (9)–(11) USING THE PARAMETERS IN TABLE 1 AND $\alpha = 4°$ AND $Pr = 1$

No.	Date; Time (LST)	Modelled z_j (m)	Modelled z_i(?) (m)	Modelled u_j (m s^{-1})
1	25/5; 17.35	5.2	24.5	7.3
2	27/5; 08.50	14.3	38.2	4.9
3	09/6; 08.36	9.1	38.7	11.5
4	11/6; 14.00	13.1	51.6	8.7
5	14/6; 11.40	11.9	46.2	6.4
6	14/6; 23.39	8.8	41.0	6.6
7	15/6; 02.38	4.6	23.9	5.6
8	07/7; 02.41	9.2	37.9	5.9
9	07/7; 05.39	3.3	16.7	3.7
10	07/7; 16.36	5.2	25.8	6.9
11	20/7; 17.33	11.7	50.3	9.9
12	21/7; 02.45	5.9	29.1	6.8
13	21/7; 05.36	12.1	45.5	5.2
14	11/8; 17.33	7.5	33.8	6.6
15	28/8; 11.31	8.0	34.6	5.4
16	28/8; 14.32	8.7	37.4	6.0

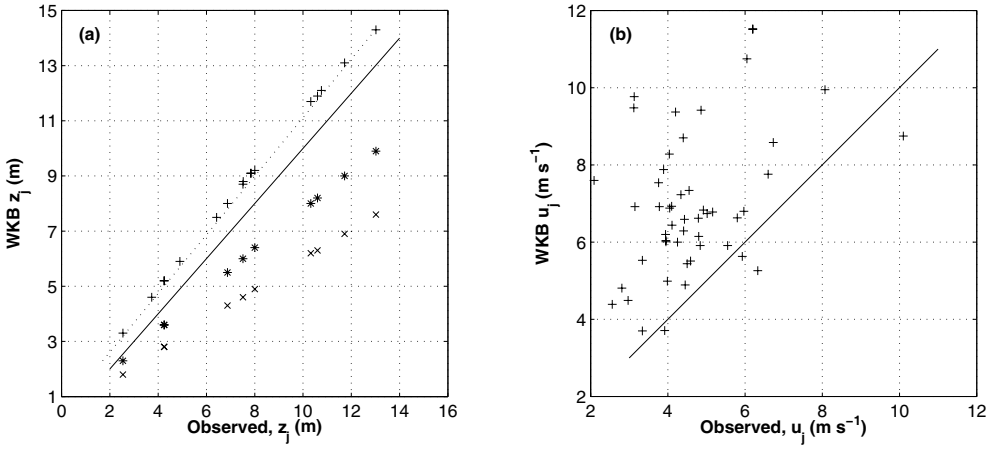

Figure 6. Scatter plots showing correspondence between observed and WKB modelled (a) jet height, z_j, from Tables 1 and 2 and (b) jet maximum speed, u_j (all data). (a) shows model values assuming Prandtl numbers 1 (+), 1.5 (∗) and 2 (×). Solid line is 1:1, dotted line is $y = 1.06x + 0.5$.

'columns' is due to the low spatial resolution of the observation mast data. Assuming that (8) holds true, we are still not able to determine C with sufficient accuracy. The same is true for γ, which is responsible for about as much of the scatter in Fig. 7 as C. The agreement in Fig. 7 lends support to the theory expressed in (8), but also calls for further investigation. The value of B found here should also be considered a first estimate, considering that the standard deviation is of the same order of magnitude as the constant itself.

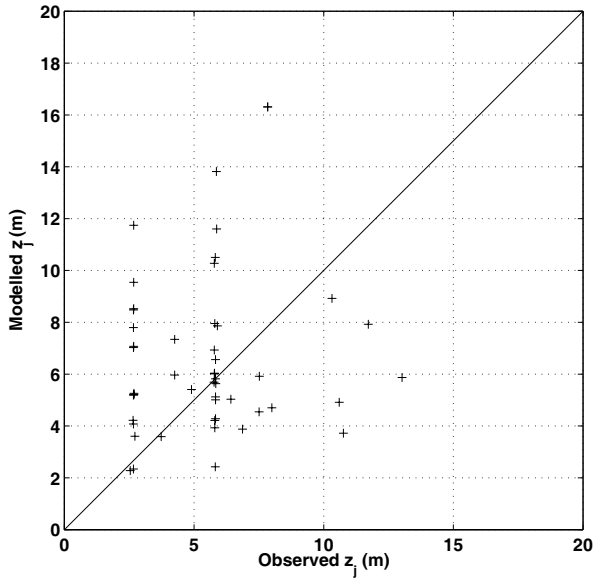

Figure 7. Observed and modelled jet height, z_j, derived from (8), using $B = 9.7 \times 10^{-4}$. The correlation coefficient is 0.07.

(*d*) *Surface fluxes*

As mentioned in the introduction, the main goal in this study is to improve our understanding of the VSBL, in particular the surface fluxes and their probable modulation of a climate signal. The relevant quantities from the Prandtl model are then the turbulent fluxes of momentum and heat. The fluxes are defined as

$$-\overline{u'w'} = u_*^2 = K_m \frac{\partial u}{\partial z}, \tag{12}$$

$$-\overline{\theta'w'} = \theta_* u_* = K_H \left(\frac{\partial \theta}{\partial z} + \gamma \right), \tag{13}$$

and are thus easily calculated from the Prandtl model. Figure 8 shows scatter plots of the momentum and heat fluxes based on observations and both the classic and improved versions of the Prandtl model, for all 50 soundings. Observed data are from the sonic anemometer on the wind mast. The constant K solutions have $K = K_{\max}/3$ (cf. GOc). Statistics for the scatter plots are given in Table 3.

Figure 8 and Table 3 show that the momentum flux modelled with the WKB solution is well oriented along the 1:1 line, while the classic Prandtl solution gives flux values which are too high. In fact, the constant K solutions are almost like noise about a more or less constant value. On the other hand, the WKB solutions, while also showing some scatter, are systematically aligned with the measurements around the 1:1 line. The momentum flux is more closely aligned with the 1:1 line than the heat flux, showing a higher correlation and a better regression slope (see Table 3). The scatter in the heat flux is a further indication of the previously noted problem of adequate determination of the temperature parameters (also see GOb). Although neither of the scatter plots in Fig. 8 can be said to show excellent agreement, it is apparent that the WKB Prandtl model constitutes a clear improvement over the constant K Prandtl model and provides an adequate way of calculating the surface fluxes.

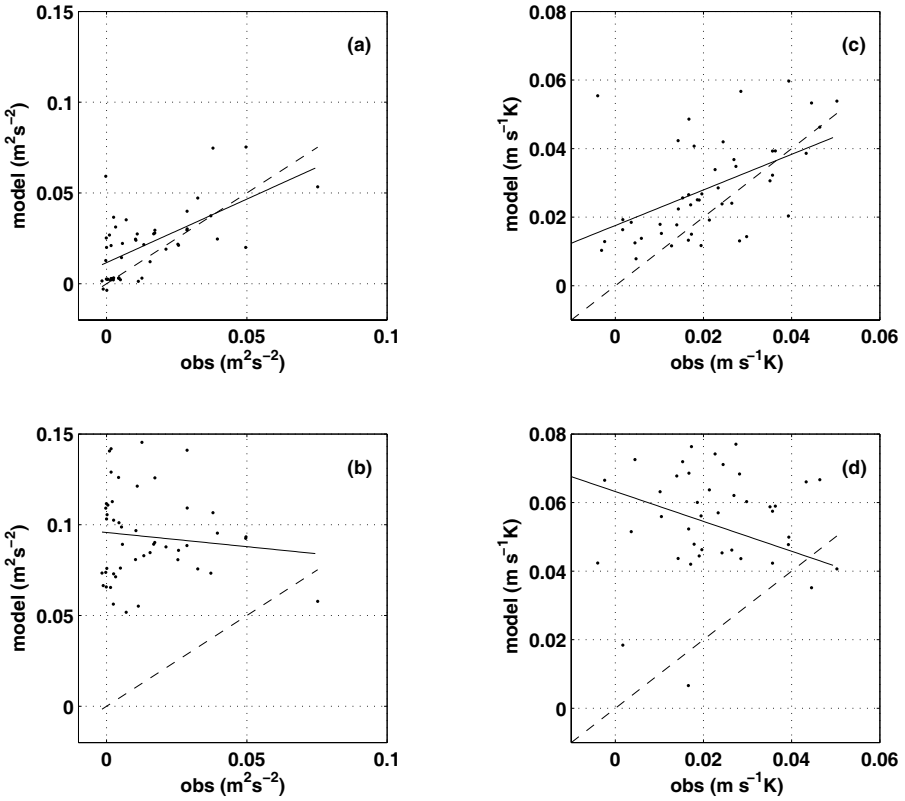

Figure 8. Scatter plots (50 data points each panel) of momentum flux, comparing measurements (from the sonic anemometer at approx. 3 m height) with (a) WKB and (b) K = constant solutions to the Prandtl model. 1:1 lines are dashed. Solid lines are the regression lines according to Table 3. (c) and (d): as (a) and (b), but for heat flux.

TABLE 3. STATISTICS FOR THE SCATTER PLOTS (FIG. 8), SHOWING EFFECTIVENESS OF WKB AND CONSTANT K PRANDTL MODELS IN CALCULATING THE MOMENTUM AND HEAT FLUXES

	Momentum flux, u_*^2				Heat flux, $\theta_* u_*$			
	r	k	m	p	r	k	m	p
WKB	0.62	0.70	0.016	2.5×10^{-4}%	0.53	0.52	0.018	9.3×10^{-3}%
K = constant	−0.11	−0.16	0.096	46%	−0.33	−0.43	0.063	2.1%

r is the correlation, k the slope, m the offset and p the probability that this correlation could have arisen by chance (calculated using the standard t-test). All calculations were performed with the commercial Matlab program.

5. DISCUSSION AND CONCLUSIONS

In this work we have compared a modified Prandtl model for katabatic flow, using variable eddy diffusivity, to observations from Breidamerkurjökull, Iceland. Using simple and conservative criteria for both mast and balloon data, we found that the katabatic flow is highly persistent. From the mast, 45% of the data agree with the katabatic criteria, whereas for the balloon data the number is 40%. The conservative nature of the criteria implies that the frequency of katabatic flow is probably higher than the numbers given here (cf. Mahrt 1982; Egger 1990).

A fair agreement was found between the improved Prandtl model solutions and observations (Fig. 6). The strength of the jet shows a considerable scatter about the observed values and is often overestimated. However, the jet height is surprisingly well aligned with the observed values. The scatter in the strength of the jet is attributed to the difficulty in accurately determining (primarily) C but also γ.

The theoretical expression (8) for the jet height, devised by Oerlemans (1998) and GOc, is compared to observed data and a first estimate for the coefficient $B = 9.7 \times 10^{-4}$ is determined. These data show a scatter around the observations that is similar to that for the strength of the katabatic jet. Since the common factor for these two parameters is a linear dependence on the temperature deficit, C, it is concluded that at least a part of the scatter is caused by uncertainties in the determination of C. Also γ was found to influence the scatter.

We conclude that the flux calculations (50 points in total) based on the theories of GOa,b are in good agreement with those observed on Breidamerkurjökull (cf. Table 3 and Fig. 8). This has two interesting and perhaps important consequences. First, the modified Prandtl model is an almost analytical way of calculating the surface fluxes in a katabatic VSBL. Second, the agreement with the observed data means that we can support the classic model by Prandtl regarding the fundamental physics, thus strengthening our understanding of the VSBL.

One may ask why there is a good agreement between the observations and a local flow theory such as the Prandtl model. Breidamerkurjökull has a long fetch zone, and this may be sufficient for the flow to be steady, the first strong assumption made in this study. More difficult to explain, however, is the importance of advection. In addition to providing steady flow, one would expect a long fetch to cause substantial advective effects on the flow. We can only conclude that our results suggest that the advective effects are weak, a feature also supported by Mahrt (1982).

Vatnajökull (and thus Breidamerkurjökull) is located in the middle of the North Atlantic storm tracks and is permanently subject to the influence of synoptic storms. Despite this, the katabatic flow remains fairly undisturbed by the larger-scale phenomena. Previous studies have shown a similar robustness of the katabatic flow to environmental disturbances (e.g. Grisogono *et al.* 1998). The Scorer parameter is a non-local tool used in linear wave theory to determine the ability of buoyancy waves to propagate in the vertical (e.g. Holton 1992; Nappo 2002). Figure 9 shows the Scorer parameter for sounding no. 1 in Table 1. If the horizontal wave number is smaller than the Scorer parameter,

$$Sc^2 = \frac{N^2}{U^2} - \frac{1}{U} \cdot \frac{\partial^2 U}{\partial z^2}, \tag{14}$$

the buoyancy waves can propagate vertically. If the wave number is larger than Sc^2, the waves decay exponentially with height. Figure 9(a) shows that Sc^2 turns negative just above the katabatic jet, thereby preventing wave transport of momentum between the katabatic layer and the atmosphere above. This effectively means that the katabatic layer is decoupled from the flow above. Figures 9(b) and (c) display the profiles of the two terms in (14), showing that the first term (buoyancy) is strictly positive and decreases from a large value in the strong surface inversion to a small constant value. The second term (wind curvature) is larger than the first and even changes sign. This term, responsible for the negative value of Sc^2, consists solely of the second derivative of the wind speed with height above the surface. Thus, it is inherent for the jet to decouple from the flow above. Similar results for Sc^2 have been implied by Grisogono *et al.* (1998), for example, and reported by Burk *et al.* (1999) in numerical studies of coastal and drainage flows.

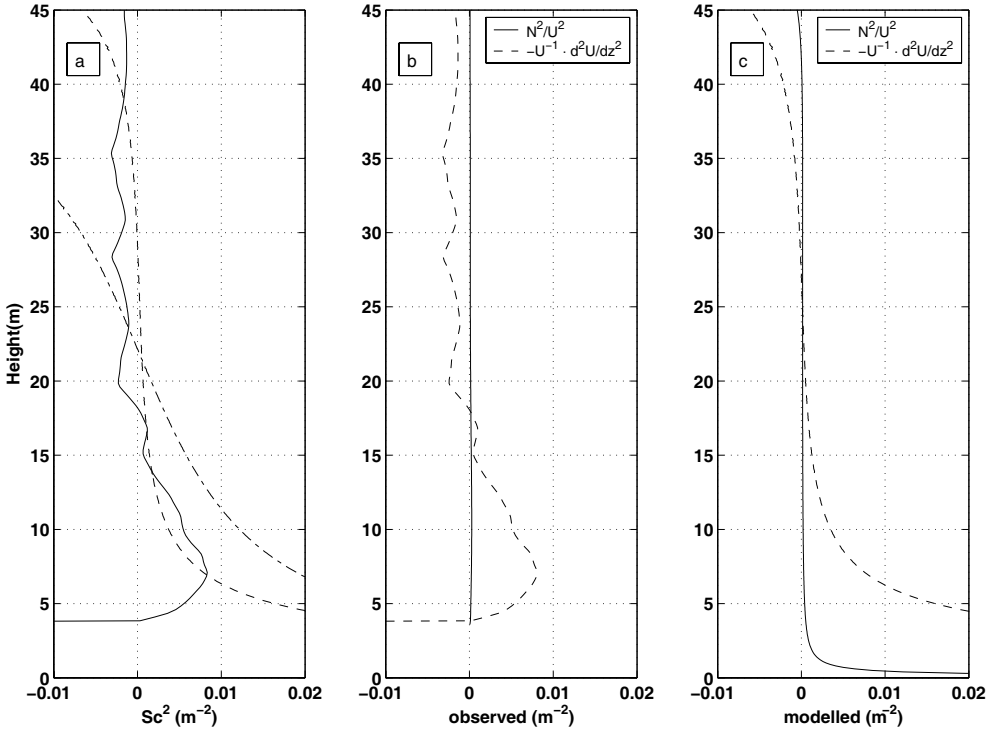

Figure 9. The Scorer parameter, Sc^2, from (14) for sounding 1 in Table 1: (a) measured (solid), constant K (dash-dotted) and WKB (dashed) solutions. The first (solid) and second (dashed) terms on the right-hand side of (14) are shown from (b) measurements and (c) the WKB solution. In the lowermost region, roughly below 5 m, the balloon observations are unreliable.

Finally, this study shows that the WKB–Prandtl model exhibits substantial improvements over the classic model, while retaining most of the latter's simplicity. There are improvements to the vertical placing and strength of the katabatic jet and also, more importantly, to the surface fluxes.

ACKNOWLEDGEMENTS

Stefan Söderberg, Michael Tjernström and Larry Mahrt are acknowledged for fruitful discussions and valuable comments on the manuscript. The comments and suggestions by two anonymous reviewers have greatly helped in improving this manuscript.

REFERENCES

Bender, C. M. and Orszag, S. A. 1999 *Advanced mathematical methods for scientists and engineers*, Springer, New York

Burk, S., Haack, T. and Samelson, R. M. 1999 Mesoscale simulation of supercritical, subcritical, and transitional flow along coastal topography. *J. Atmos. Sci.*, **56,** 2780–2795

Defant, F. 1949 Zur theorie der hangwinde, nebst bemerkungen zur theorie der berg- und talwinde. *Arch. Meteorol. Geophys. Bioklim.*, **A1,** 421–450

Denby, B. 1999 Second-order modeling of turbulence in katabatic flows. *Boundary-Layer Meteorol.*, **92,** 67–100

Egger, J. 1990 'Thermally forced flows: Theory'. Pp. 43–57 in *Atmospheric Processes over complex terrain*. Ed. W. Blumen, American Meteorological Society, Boston, USA

Emery, W. J. and Thompson, R. E. 1997 *Data analysis methods in physical oceanography.* Pergamon Elsevier, Oxford, UK

Grisogono, B. 2003 Post-onset behaviour of the pure katabatic flow. *Boundary-Layer Meteorol.*, **107,** 157–175

Grisogono, B. and Oerlemans, J. 2001a Katabatic flow: analytic solution for gradually varying eddy diffusivities. *J. Atmos. Sci.*, **58,** 3349–3354

2001b A theory for the estimation of surface fluxes in simple katabatic flows. *Q. J. R. Meteorol. Soc.*, **127,** 2725–2739

2002 Justifying the WKB approximation in pure katabatic flows. *Tellus*, **54A,** 453–462

Grisogono, B., Ström, L. and Tjernström, M. 1998 Small-scale variability in the coastal atmospheric boundary layer. *Boundary-Layer Meteorol.*, **88,** 23–46

Holton, J. R. 1992 *An Introduction to Dynamic Meteorology*, (third ed.), Academic Press, UK

Mahrt, L. 1982 Momentum balance of gravity flows. *J. Atmos. Sci.*, **39,** 2701–2711

1998 Stratified atmospheric boundary layers and breakdown of Models. *Theor. Comp. Fluid Dyn.*, **11,** 263–279

Munro, D. S. 1989 Surface roughness and bulk heat transfer on a glacier. *J. Glaciol.*, **35,** 343–348

Munro, D. S. and Davies, J. A. 1978 On fitting the log-linear model to wind speed and temperature profiles over a melting glacier. *Boundary-Layer Meteorol.*, **15,** 423–437

Nappo, C. J. 2002 *An Introduction to Atmospheric Gravity Waves.* Academic Press, San Diego

Oerlemans, J. 1998 'The atmospheric boundary layer over melting glaciers'. Pp. 129–153 in *Clear and Cloudy Boundary Layers.* Eds. A. A. M. Holtslag and P. G Duynkerke, Royal Netherlands Academy of Arts and Sciences, The Netherlands

2001 *Glaciers and climate change.* A.A. Balkema, Lisse, The Netherlands

Oerlemans, J. and Grisogono, B. 2002 Glacier winds and parameterisation of the related surface heat fluxes. *Tellus*, **54A,** 440–452

Oerlemans, J., Björnsson, H., Kuhn, M., Obleitner, F., Palsson, F., Smeets, C. J. P. P., Vugts, H. F. and De Wolde, J. 1999 Glacio-meteorological investigations on Vatnajökull, Iceland, summer 1996: An overview. *Boundary-Layer Meteorol.*, **92,** 3–26

Pahlow, M., Parlange, M. B. and Porté-Agel, F. 2001 On Monin-Obukhov similarity in the stable atmospheric boundary layer. *Boundary-Layer Meteorol.*, **99,** 225–248

Prandtl, L. 1942 *Führer durch die Strömungslehre.* Vieweg und Sohn, Braunschweig, Germany

Skyllingstad, E. D. 2003 Large-eddy simulation of katabatic flows. *Boundary-Layer Meteorol.*, **106,** 217–243

Smeets, C. J. P. P., Duynkerke, P. G. and Vugts, H. F. 1999 Observed wind profiles and turbulence fluxes over an ice surface with changing surface roughness. *Boundary-Layer Meteorol.*, **92,** 101–123

Stull, R. B. 1988 *An Introduction to Boundary Layer Meteorology.* Kluwer Academic Publishers, Dordrecht, The Netherlands

van der Avoird, E. and Duynkerke, P. G. 1999 Turbulence in a katabatic flow. Does it resemble turbulence in stable boundary layers over flat surfaces? *Boundary-Layer Meteorol.*, **92,** 39–66